SCIENTIFIC REPORTS

OPEN

SUBJECT AREAS:
MAGNETIC PROPERTIES AND MATERIALS
CONDENSED-MATTER PHYSICS

Received
8 January 2014

Accepted
25 February 2014

Published
14 March 2014

Correspondence and requests for materials should be addressed to J.H. (hongj@pknu.ac.kr)

Metal free half metallicity in 2D system: structural and magnetic properties of g-C_4N_3 on BN

Arqum Hashmi & Jisang Hong

Department of Physics, Pukyong National University, Busan 608-737, Korea.

Synthesis of a half metallic material on a substrate is highly desirable for diverse applications. Herein, we have investigated structural, adsorptive, and magnetic properties of metal free graphitic carbon nitride (g-C_4N_3) layer on hexagonal BN layer (h-BN) using the optB88-vdW van der Waals density functional theory. It is found that g-C_4N_3 layer can be adsorbed on BN layer due to the change of lattice constant of the hybridized system. The newly found lattice constant of g-C_4N_3 was 9.89 Å, which is approximately 2% lower and larger than to those of free standing BN and g-C_4N_3, respectively. Also, 2 × 2 surface reconstruction geometry predicted in free standing g-C_4N_3 layer disappears on the BN layer. Interestingly, we have found that metal free half metallic behavior in g-C_4N_3 can be preserved even on BN layer and the characters of spin polarized planar orbitals suggest that our theoretical prediction can be verified using normal incidence of K-edge X-ray magnetic circular dichroism (XMCD) measurement.

3d transition metal elements are believed to be essential to introduce magnetism. However, many studies showed that magnetism could occur in the absence of the 3d transition metal elements and it is referred to as d^0 magnetism. Examples of d^0 magnetism from various types of oxide materials[1,2] and semiconductors[3,4] have been reported and in most of discussions the d^0 magnetism is attributed to the effect of vacancy defects or lattice distortion. Half metallic magnetism also received great research interest because half metallic materials have various potential applications in spintronics. In most of previous studies on half metallic systems, the combination of various types of materials with 3d transition metal elements has been investigated[5,6]. Besides the magnetism of conventional 3d systems, 2p electron systems also yield another interesting property. Usually, 2p electron systems are known to display non-magnetic behavior in bulk state. Nonetheless, further studies in two dimensional structures have indicated that magnetic state is likely to be achieved in low dimensional geometry. For instance, many reports have shown the development of magnetic state in graphene or BN; the influence of vacancy defect or adatom defect has been discussed[7,8]. Here, the local magnetic moment has been discussed in most cases.

For spintronics, it is of interest to examine ferromagnetism in pure 2p electron systems in the absence of transition metal elements because large spin relaxation time is expected owing to the relatively weak spin-orbit coupling. Hence, the investigation of biocompatible material with half metallic properties of particular interest. Among various candidates, C-N based materials show great potential. In this respect, considerable efforts have been devoted to polymetric graphitic carbon nitride (g-C_3N_4)[9–11]. This structure features intrinsic vacancies that are expected to produce spin polarized state. However, g-C_3N_4 displays non-magnetic properties. Recently, a similar material g-C_4N_3 in the framework of g-C_3N_4 has been synthesized[12]. This metal free material showed half metallic properties in the free standing state, as reported by Du *et al*[13–16]. Additionally, the authors claimed that the g-C_4N_3 has a (2 × 2) surface reconstructed geometry due to a buckling feature in the free standing layer.

It is highly desirable to synthesize of a half metallic material on a substrate for diverse applications because one can avoid various difficulties of manipulating free standing layer. It is therefore necessary to choose a supporting material that does not disturb the intrinsic half metallic properties of g-C_4N_3. However, investigation of half metallic properties of metal-free g-C_4N_3 on a supporting material has yet to be reported. Herein, we for the first time investigate structural, adsorption, and magnetic properties of g-C_4N_3/BN.

Vienna ab initio simulation package (VASP) was used. Herein, the van der Waals interaction was included. In particular, van der Waals interaction of optB88-vdW method[17–19] was employed to investigate the physical properties of g-C_4N_3/BN. A vacuum distance of 15 Å was applied along the perpendicular direction to the film surface. All calculations were performed based on using 9 × 9 × 1 k-points and a kinetic energy of 700 eV cutoff.

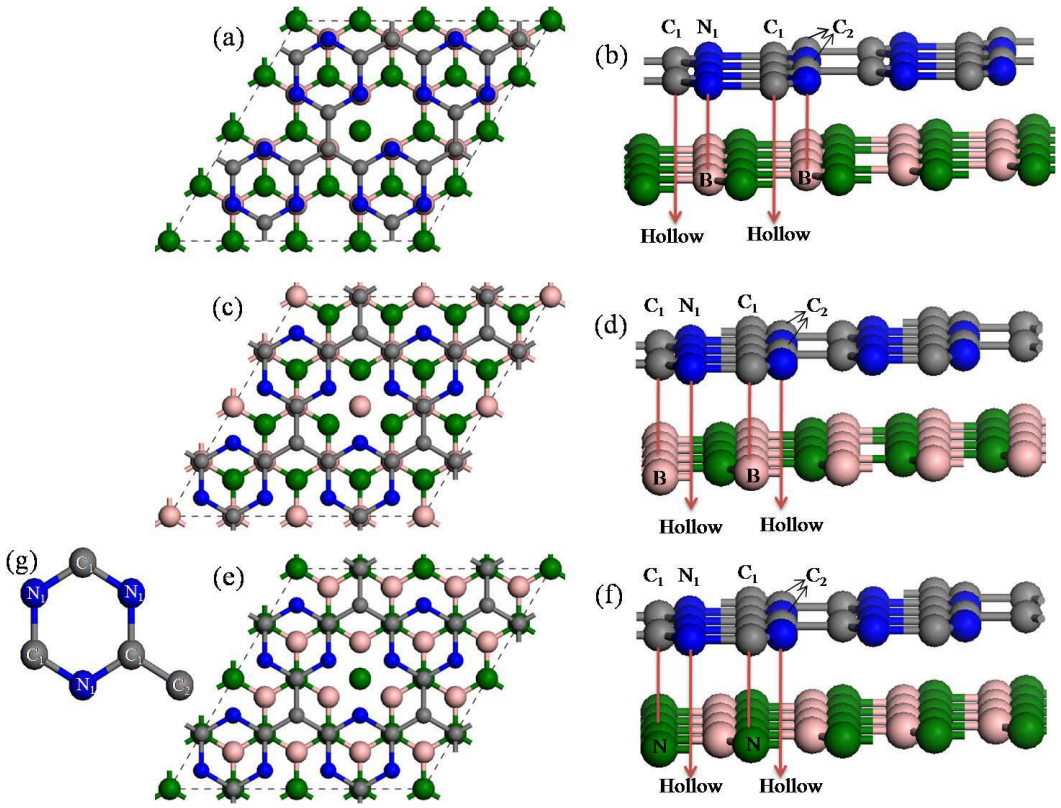

Figure 1 | Schematic illustrations of top and side views for adsorption structure. (a)–(b) C_1 on top of BN hollow and N_1 and C_2 on top B (c)–(d) C_1 on top of B and N_1 and C_2 on top of BN hollow (e)–(f) C_1 on top of N belonged to BN layer and N_1 and C_2 on top of BN hollow (g) (1×1) structure of *g*-C_4N_3.

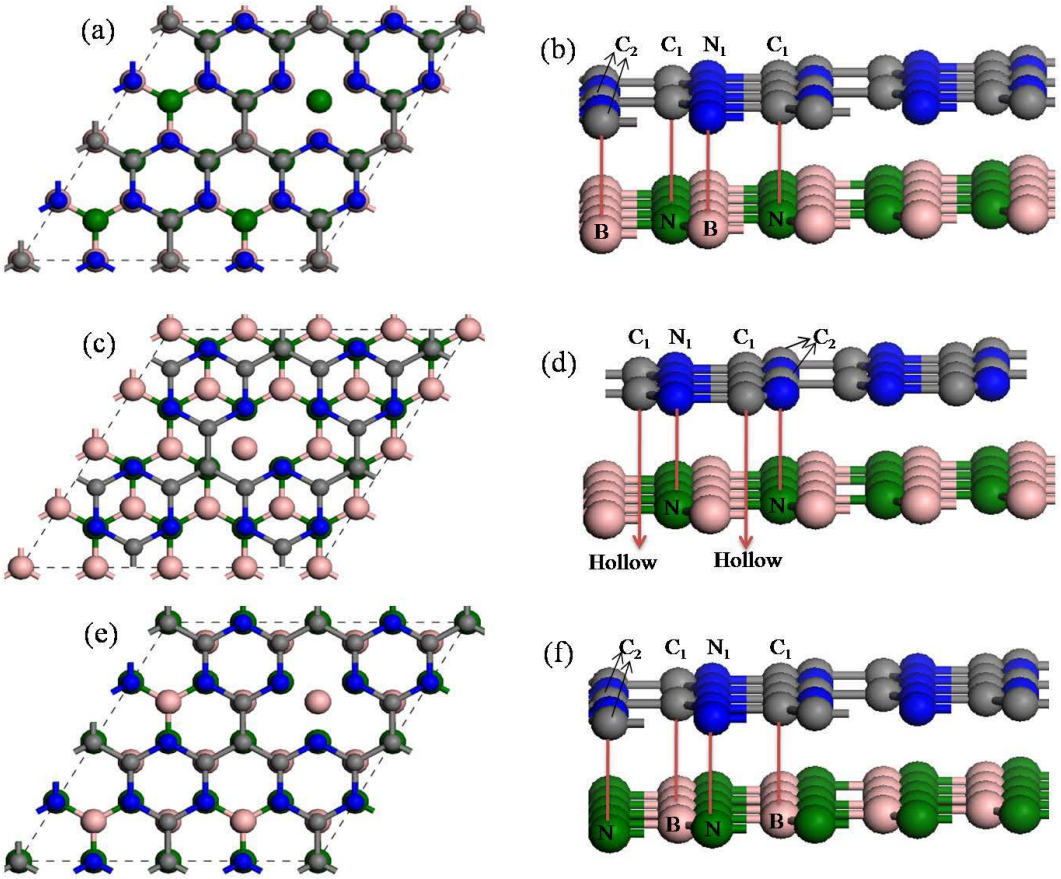

Figure 2 | Schematic illustrations of top and side views for adsorption structure. (a)–(b) C_1 on top of N belonged to BN layer and N_1 and C_2 on top of B (c)–(d) C_1 on top of hollow and N_1 and C_2 on top of N (e)–(f) C_1 on top of B and N_1 and C_2 on top of N.

Table I | Calculated total energy Difference (in meV) and interlayer distances (in Å) in each configuration

structure	(a)	(b)	(c)	(d)	(e)	(f)
FM	0	65	139	161	282	324
AFM	177	258	352	351	570	551
interlayer distance	3.18	3.25	3.28	3.31	3.39	3.44

The most stable lattice constant of g-C_4N_3/BN was investigated by calculating the total energy as a function of lattice parameter. For the adsorptive and magnetic properties of hybridized g-C_4N_3/BN system, we have considered a (2 × 2) g-C_4N_3 layer onto a (4 × 4) BN layer. Structure optimization was performed via force and energy minimization process. In addition, ferromagnetic (FM), antiferromagnetic (AFM) and non-magnetic spin configurations were considered for the magnetic ground state. It is worth noting that the lattice constant of (1 × 1) g-C_3N_4 unit cell is 4.74 Å, but that of (1 × 1) g-C_4N_3 is 4.84 Å. Moreover, the g-C_4N_3 is known to have a (2 × 2) reconstructured surface geometry, thus the ground state lattice constant becomes 9.68 Å. This suggests that the lattice constant of g-C_4N_3 is likely to be modified in the presence of external effect. Consequently, we will explore the most stable lattice structure of g-C_4N_3/BN hybridized system by changing its lattice constant.

Fig. 1 and Fig. 2 show the schematic configurations of g-C_4N_3/BN systems featuring 6 different adsorption sites. The green and pink spheres represent the N, B atom in BN layer, respectively, while the gray and blue spheres represent the C and N atoms in g-C_4N_3 layer, respectively. The (1 × 1) unit cell of g-C_4N_3 is depicted in Fig. 1(g); the C and N atoms that are located on the hexagonal ring are referred as C_1 and N_1, respectively, whereas C atom located outside the ring is denoted as C_2. It should be noted that the bridge adsorption site is not observed because the atoms orient themselves into the configuration shown in Fig. 1(b), regardless of the initial calculations. Table I presents the calculated total energy differences among ferromagnetic (FM) and antiferromagnetic (AFM) spin arrangements, and the distances between BN and g-C_4N_3 layers. The results were based on the most stable lattice constant. The total energy for configuration depicted in Fig. 1(a) was set to zero as a reference energy that produced the most stable system. The interlayer distance for this configuration was 3.18 Å. Interestingly, the FM ground state was still preserved even in the BN underlayer, and was independent of the adsorption sites. It is worth noting that the energy difference for configuration 1(a) between FM and non-magnetic states was 278 meV. Fig. 3 shows the total energy curve as a function of the

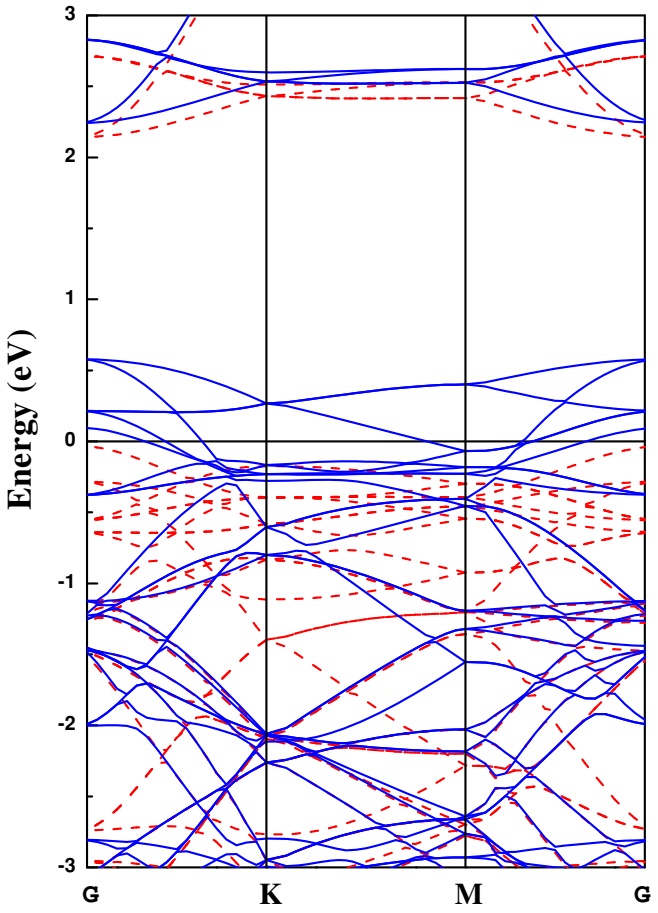

Figure 4 | Electronic band structure along high symmetry directions. The blue and red lines represent majority and minority spin bands respectively. The black horizontal line denotes the Fermi level.

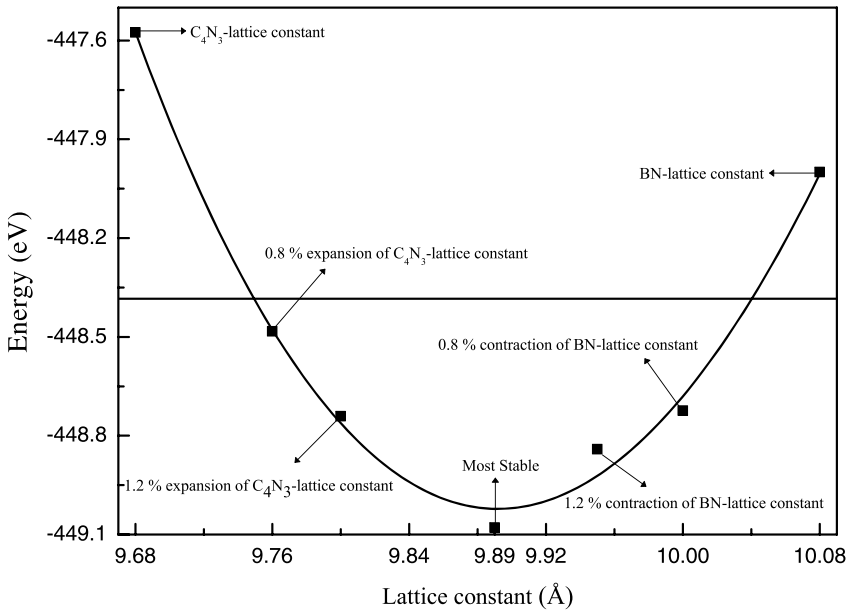

Figure 3 | Calculated total energy as a function of lattice constant.

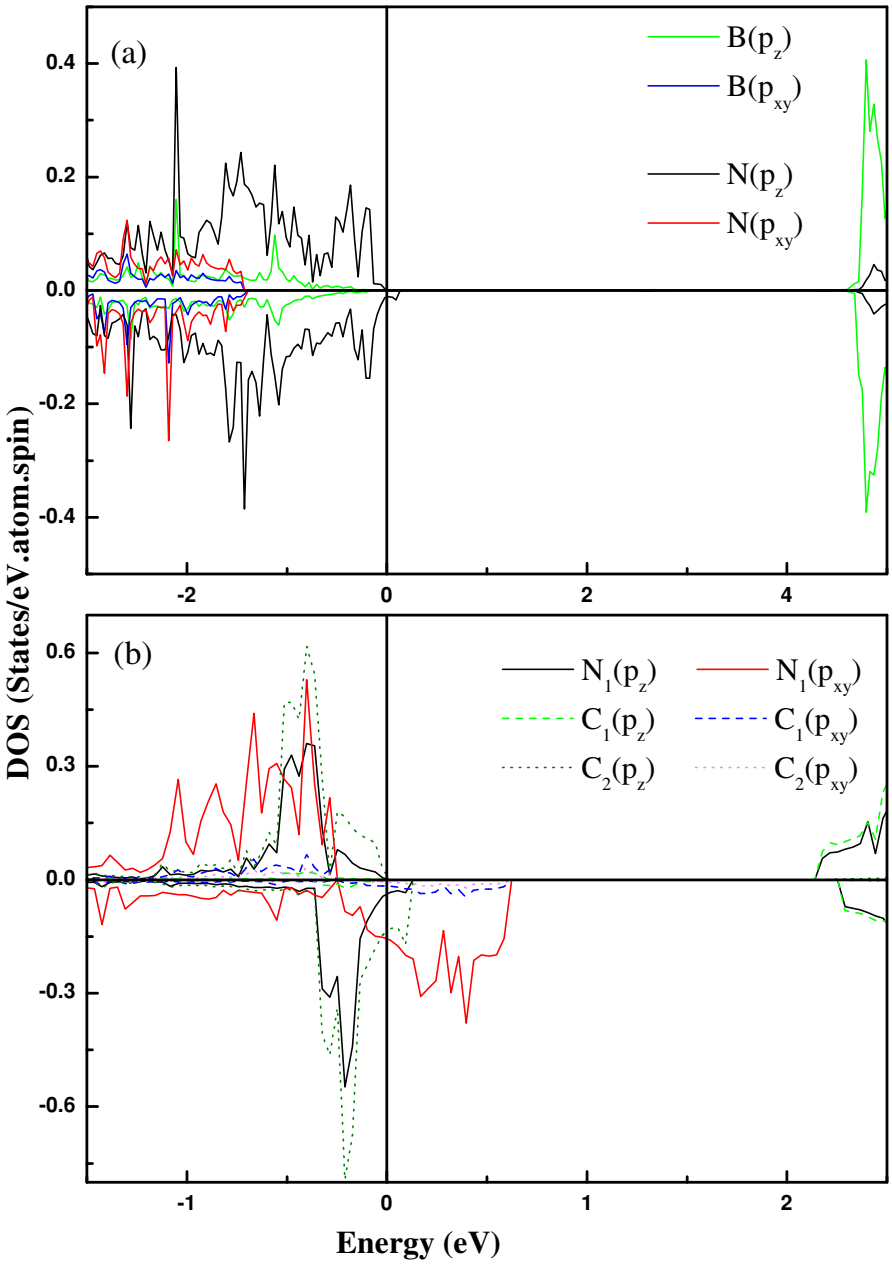

Figure 5 | **Calculated m-DOS of (a) B and N atoms in BN layer (b) C and N atoms in *g*-C_4N_3 layer.**

lattice constant for the configuration Fig. 1(a) in which the ground state was realized. The solid line represents the fitting curve obtained with a parabolic polynomial function. A total energy minimum was observed at a lattice constant of 9.89 *Å*. The ideal monolayer of BN in a (4 × 4) unit cell has a lattice constant of 10.08 *Å* and that of free standing *g*-C_4N_3 in a (2 × 2) unit cell is 9.68 *Å*. Therefore, a newly found lattice constant of *g*-C_4N_3 was 9.89 *Å*, which is approximately 2% lower and larger than to those of free standing BN and *g*-C_4N_3, respectively.

We now discuss the adsorption energy. The adsorption energy (E_{ads}) was calculated as: $E_{ads} = E_{BN} + E_{C_4N_3} - E_{C_4N_3/BN}$, where E_{BN} and $E_{C_4N_3}$ denote the total energies of the free standing systems, and $E_{C_4N_3/BN}$ represents the total energy of the hybridized system. To calculate the total energy of free standing layers, the corresponding lattice constants of (2 × 2) unit cell for *g*-C_4N_3 and (4 × 4) unit cell for BN were used. The calculated total energies of the free standing BN and *g*-C_4N_3 are 248.685 eV and 199.699 eV, respectively. The horizontal line in Fig. 2 represents the sum of the energies of the free standing systems, *i.e.* $E_{BN} + E_{C_4N_3}$. Thus, the total energy of the *g*-C_4N_3/BN hybridized system should be below the horizontal line. Based on the calculated total energy curve in Fig. 3, the *g*-C_4N_3/BN hybridized system is unstable when the *g*-C_4N_3/BN structure has a lattice constant similar to that of either BN or *g*-C_4N_3 because the resulting total energy is larger than the sum of the free standing systems energies. The total energy minimum of the hybridized system was obtained at a lattice constant of 9.89 *Å*, which corresponds to a 2% contraction and expansion with respect to that of BN and *g*-C_4N_3, respectively. The ground state lattice constant obtained herein is comparable with the calculated average of the respective lattice constants of the free standing *g*-C_4N_3 and BN layers; the lattice changes enables adsorption of *g*-C_4N_3 layer on the BN layer. The calculated adsorption energy was 0.67 eV. Another interesting aspect is the structural behavior of the *g*-C_4N_3/BN system. According to previous theoretical prediction[13], the free standing

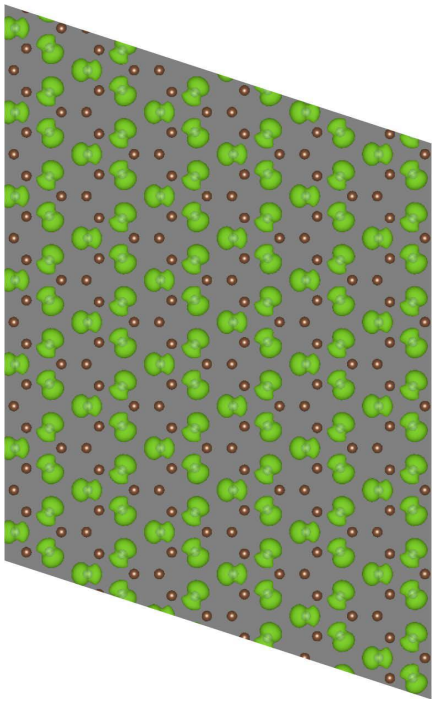

Figure 6 | Calculated spin charge density.

g-C_4N_3 surface is believed to show a (2×2) reconstructed geometry owing to surface buckling. However, herein, we observed that the surface reconstruction is absent on the BN layer and the g-C_4N_3 layer becomes flat layer with the interlayer spacings presented in Table I. We have found using Bader charge analysis[20–23] that no significant charge transfer takes place between two layers. However, the van der Waals interaction between these two layers significantly influences the surface structure. Owing to this geometric effect, the lattice constant of g-C_4N_3/BN will be 4.945 $\AA$ in a (1×1) unit cell.

For the configuration depicted in Fig. 1(g), magnetic moments of N_1 and C_2 are 0.26 μ_B and 0.028 μ_B, respectively. The calculated total magnetic moment per unit cell is 4 μ_B, indicating the half metallic nature of g-C_4N_3. Fig. 4 shows the electronic band structure. The valence bands of majority spin states are located below the Fermi level, whereas the minority spin bands cross the Fermi level. These finding confirms that the half metallic nature of the metal free g-C_4N_3/BN system. Fig. 5(a) and (b) show the m-resolved density of states (m-DOS). As observed, the spin polarized state mainly originates from the $p_{x,y}$ orbitals of the N_1 atoms in the g-C_4N_3 layer. In contrast, no significant spin polarization was found in the p_z orbital. Moreover, this result indicates that the top of the valence involves the planar $p_{x,y}$ orbitals. Fig. 6 illustrates the calculated spin polarized charge density of g-C_4N_3/BN. As inferred, the planar $p_{x,y}$ orbitals contribute to the magnetic moment. Additionally, observed spin polarization in planar orbitals indicates that the K-edge X-ray magnetic circular dichroism (XMCD) measurment, using normal incidence beam, can verify our predictions because the magnetism of g-C_4N_3/BN originates from the $2p_{x,y}$ orbital. In contrast, no XMCD signals would be detected with a grazing incidence beam because the selection $\Delta m = \pm 1$ is not satisfied.

In conclusion, we explored adsorption, structural, and magnetic properties of g-C_4N_3/BN. The hybridized system had a new lattice constant, which is different from those of free standing BN and g-C_4N_3 layers and this lattice change was responsible for adsorption of g-C_4N_3 on BN layer. In addition, the surface reconstruction feature found in free standing layer disappeared due to the interaction with BN layer. The magnetic moment arises from the N atoms in g-C_4N_3 layer, whereas the C atoms show almost negligible spin polarization. Very interestingly, half metallic behavior is preserved even on BN layer and the half metallicity originates mainly from the $2p_{x,y}$ planar orbitals of N atoms in g-C_4N_3 layer. We suggest that this spin polarization from $2p_{x,y}$ orbitals can be verified with the K-edge XMCD measurement using normal incidence beam. Overall, this metal free half metallic behavior even on a supporting material will enable the development of new and intriguing properties that show potential for next generation spintronics.

1. Venkatesan, M., Fitzgerald, C. B. & Coey, J. M. D. Unexpected magnetism in a dielectric oxide. *Nature* **430**, 630 (2004).
2. Kim, D., Yang, J. & Hong, J. Ultrathin half metallic N and antiferromagnetic semiconducting C layers on MgO(001). *J. Phys. Condens. Matter* **22**, 486006 (2010).
3. Hong, N. H., Sakai, J., Poirot, N. & Brize, V. Room-temperature ferromagnetism observed in undoped semiconducting and insulating oxide thin films. *Phys. Rev. B* **73**, 132404 (2006).
4. Kim, D., Hong, J., Park, Y. & Kim, K. The origin of oxygen vacancy induced ferromagnetism in undoped TiO_2. *J. Phys. Condens. Matter* **21**, 195405 (2009).
5. Du, C. *et al*. Control of Magnetocrystalline Anisotropy by Epitaxial Strain in Double Perovskite Sr2FeMoO6 Films. *Phys. Rev. Lett.* **110**, 147204 (2013).
6. deGroot, R. A., Mueller, F. M., van Engen, P. G. & Buschow, K. H. J. New class of materials: Half-metallic ferromagnets. *Phys. Rev. Lett.* **50**, 2024–2027 (1983).
7. Yang, J., Kim, D., Hong, J. & Qian, X. Magnetism in boron nitride:Adatom and vacancy defect. *Surf. Sci.* **604**, 1603–1607 (2010).
8. Si, M. S. & Xue, D. S. Magnetic properties of vacancies in a graphitic boron nitride sheet by first-principles pseudopotential calculations. *Phys. Rev. B* **75**, 193409 (2007).
9. Stolbov, S. & Zuluaga, S. Sulfur doping effects on the electronic and geometric structures of graphitic carbon nitride photocatalyst: insights from first principles. *J. Phys. Condens. Matter.* **25**, 085507 (2013).
10. Wei, W. & Jacob, T. Strong excitonic effects in the optical properties of graphitic carbon nitride g-C3N4 from first principles. *Phys. Rev. B.* **87**, 085202 (2013).
11. Wang, X. *et al*. A metal-free polymeric photocatalyst for hydrogen production from water under visible light. *Nat. Materials.* **8**, 76–80 (2009).
12. Lee, J. S., Wang, X., Luo, H. & Dai, S. Fluidic Carbon Precursors for Formation of Functional Carbon under Ambient Pressure Based on Ionic Liquids. *Adv. Mater.* **22**, 1004–1007 (2010).
13. Du, A., Sanvito, S. & Smith, S. C. First-Principles Prediction of Metal-Free Magnetism and Intrinsic Half-Metallicity in Graphitic Carbon Nitride. *Phys. Rev. Lett.* **108**, 197207 (2012).
14. Li, X., Zhou, J., Wang, Q., Kawazoe, Y. & Jena, P. Patterning Graphitic C-N Sheets into a Kagome Lattice for Magnetic Materials. *J. Phys. Chem. Lett.* **4**, 259–263 (2013).
15. Li, X., Zhang, S. & Wang, Q. Stability and physical properties of a tri-ring based porous g-C4N3 sheet. *Phys. Chem. Chem. Phys.* **15**, 7142–7146 (2013).
16. Wu, M., Wang, Q., Sun, Q. & Jena, P. Functionalized Graphitic Carbon Nitride for Efficient Energy Storage. *J. Phys. Chem. C.* **117**, 6055–6059 (2013).
17. Dion, M., Rydberg, H., Schroder, E., Langreth, D. C. & Lundqvist, B. I. Van der Waals Density Functional for General Geometries. *Phys. Rev. Lett.* **92**, 246401 (2004).
18. Graziano, G., Klimes, J., Fernadez-Alonso, F. & Michaelides, A. Improved description of soft layered materials with van der Waals density functional theory. *J. Phys. Condens. Matter.* **24**, 424216 (2012).
19. Liu, W. *et al*. Benzene adsorbed on metals: Concerted effect of covalency and van der Waals bonding. *Phys. Rev. B.* **86**, 245405 (2012).
20. Bader, R. F. W. *Atoms in Molecules: A Quantum Theory* (Oxford University Press, 1990).
21. Henkelman, G., Arnaldsson, A. & Jonsson, H. A fast and robust algorithm for Bader decomposition of charge density. *Comput. Mater. Sci.* **36**, 354–360 (2006).
22. Sanville, E., Kenny, S. D., Smith, R. & Henkelman, G. Improved grid-based algorithm for Bader charge allocation. *J. Comput. Chem.* **28**, 899–908 (2007).
23. Tang, W., Sanville, E. & Henkelman, G. A grid-based Bader analysis algorithm without lattice bias. *J. Phys. Condens. Matter.* **21**, 084204–084207 (2009).

Acknowledgements

This research was supported by Basic Science Research Program through the National Research Foundation of Korea(NRF) funded by the Ministry of Education, Science and Technology(No. 2013R1A1A2006071).

Author contributions

J.H. reviewed and wrote the manuscript. A.H. prepared figures 1–6.

Additional information

Competing financial interests: The authors declare no competing financial interests.

How to cite this article: Hashmi, A. & Hong, J. Metal free half metallicity in 2D system: structural and magnetic properties of g-C_4N_3 on BN. *Sci. Rep.* **4**, 4374; DOI:10.1038/srep04374 (2014).